Results in Optics 17 (2024) 100750

Contents lists available at ScienceDirect

Results in Optics

journal homepage: www.sciencedirect.com/journal/results-in-optics

Intense violet electroluminescence of thin SiO_2 layers with SnO_2 nanocrystals

Ivan Romanov [a], Irina Parkhomenko [a,*], Liudmila Vlasukova [a], Elke Wendler [b], Fadei Komarov [c]

[a] Belarusian State University, Kurchatov Ave. 5, 220045 Minsk, Belarus
[b] Institute for Solid State Physics, Friedrich-Schiller-University Jena, Max-Wien-Platz 1, D-07743 Jena, Germany
[c] A. N. Sevchenko Institute of Applied Physical Problems of Belarusian State University, Kurchatov Ave. 7, 220045 Minsk, Belarus

ARTICLE INFO

Keywords:
Silica layers
Ion implantation
Tin dioxide
Nanocrystals
Electroluminescence
Quantum efficiency

ABSTRACT

It has been shown that Sn implantation with subsequent annealing in air leads to an increase in the electroluminescence (EL) intensity of SiO_2/Si structure by two orders of magnitude. Intense violet EL with a maximum at 3.21 eV was observed at room temperature by the naked eye at forward bias. The observed emission was attributed to radiative recombination in SnO_2 nanocrystals synthesized in SiO_2 layers. The external quantum efficiency (EQE) increased with decreasing Sn concentration The maximum external quantum efficiency was found to be 0.7 % for the silica film Sn-implanted at the lowest fluence of 2.5×10^{16} cm^{-2}. The non-radiative charge transport (shunt current) through the sample and mechanism of EL excitation are discussed. It has been concluded that the Poole–Frenkel mechanism, or tunneling between traps are the most likely mechanisms of charge transport to light-emitting centers.

1. Introduction

The creation of Si-based light-emitting diodes (LED) remains a key task in the development of silicon photonics. Some approaches have been proposed to deposit light-emitting nanomaterials such as GaN (Hikosaka et al., 2014; Lee et al., 2020; Cho et al., 2021), Ga_2O_3 (Huang et al., 2021), ZnO (Liu et al., 2020; Jiang et al., 2014), perovskite $CsPbBr_3$ (Xiang et al., 2023), and GeSn (Wu et al., 2023) on Si substrates. Unfortunately, the deposition of light-emitting films on Si wafers is often complicated, expensive, and resource-intensive process. On the other hand, ion implantation is a well-established technique used in the Si industry to create light-emitting centers or nanocrystals in Si or Si-based matrices such as SiO_x and SiN_x. Light-emitting Si-based layers fabricated via this approach have been demonstrated in Refs (Li et al., 2021; Koubisy et al., 2020; Nikolskaya et al., 2020; Arai et al., 2009; Zatsepin et al., 2016). The commonly used method for the analysis of the light-emitting properties of such films is photoluminescence (PL). However, for a technological application, electroluminescence (EL) is more important analytical technique. In comparison with photoluminescence, it is more difficult to excite a strong luminescence electrically. As a result, the literature data on the EL analysis of Si-based dielectric layers with demonstration of the important practical characteristics such as external quantum efficiency, threshold voltage, and current density required to initiate emission are scarce and insufficient (Fujimoto et al., 2020; Rebohle et al., 2014; Martinelli et al., 2003; Jambois et al., 2007).

Silicon dioxide is an ideal matrix for creating visible LEDs compatible with current silicon technology. To date, the implantation with various types of ions has been tested to improve the light-emitting properties of SiO_2. However, the brightest blue-violet luminescence was registered for the SiO_2/Si samples implanted with isovalent ions (Si^+, Ge^+, Sn^+) (Lopes et al., 2005; Rebohle et al., 2000; Bregolin et al., 2009; Shcheglov et al., 1995; Romanov et al., 2019; Romanov et al., 2022; Zatsepin et al., 2012; Rebohle et al., 2002; Lopes et al., 2006; Rebohle et al., 2000; Gong et al., 2016; Huang et al., 2011). There are many studies devoted to the origin of this luminescence. The similarity of the spectra regardless of the type of ion indicates the defect-related origin of the luminescence (Lopes et al., 2005; Rebohle et al., 2002; Rebohle et al., 2000; Huang et al., 2011). Namely, the PL band at 3,2 eV was interpreted as due to a $T_1 \rightarrow S_0$ transition of an oxygen deficiency center (ODC). The probability of such transition increased via enhancement of the spin–orbit coupling at substitution of Si atoms by heavier isoelectronic atoms. On the other hand, implantation with subsequent annealing can result in the synthesis of light-emitting nanocrystals. In particular, the nanocrystalline tin dioxide also emits in the violet range (Romanov et al., 2019;

* Corresponding author.
E-mail address: parhomir@yandex.by (I. Parkhomenko).

https://doi.org/10.1016/j.rio.2024.100750
Received 31 May 2024; Received in revised form 12 September 2024; Accepted 10 October 2024
Available online 11 October 2024

Romanov et al., 2022; Huang et al., 2011; Tagliente et al., 2009) by breaking the dipole-forbidden rule in the case of nanostructures (Li et al., 2012). Thus, Sn-implanted silica layers are promising material for creating violet LEDs, but the mechanisms of enhancing their luminescence still need to be studied.

To date, electroluminescence from silicon dioxide layers implanted with tin ions has been studied in (Romanov et al., 2022; Rebohle et al., 2002; Rebohle et al., 2000). To the best of our knowledge, the measured power efficiency of the Sn-implanted silica devices was reported in the Ref (Rebohle et al., 2002). It amounted to 2.5×10^{-4}. In this study, we have estimated the value of external quantum efficiency as well as have analyzed the mechanisms of charge transfer and radiative recombination in implanted SiO_2 layers when excited by an electric field. Here, the effect of Sn concentration in SiO_2 matrix on practically important parameters, such as EL in absolute values of the spectral radiant exitance, external quantum efficiency, and threshold current density to initiate emission are explored for the first time. The aim of our work is also to analyze the mechanisms of charge transfer and radiative recombination in implanted layers upon excitation by an electric field. This is an undoubtedly important step forward in the development of blue-violet Si-based nano-LEDs.

2. Material and methods

The (2×2 cm^2) samples were cut from a thermally oxidized p-type boron-doped Si substrate with SiO_2 thickness of 130 nm. These samples were implanted with 80-keV Sn ions at fluences of 2.5×10^{16}, 5×10^{16} and 1×10^{17} cm^{-2} at room temperature (RT) and annealed at 900 °C for 60 min in air ambient.

The Sn distribution in the implanted samples was calculated using SRIM-2013 (Ziegler et al., 2010). The fluence in the range of 2.5×10^{16} – 10^{17} cm^{-2} lead to a peak concentration of the implanted ions between 2.5×10^{21} – 3×10^{22} cm^{-3} (9 % – 37 at.%). The ion average projective range is about 49 nm.

The structural investigations were carried out by high-resolution transmission electron microscopy (HRTEM) using a JEOL JEM 2100 transmission electron microscope operating at 200 keV.

Fig. 1 shows the experimental setup for EL measurements in the electrolyte–dielectric–semiconductor (EDS) system. EL spectra were registered at room temperature in the range of 1.75 – 3.76 eV (710 – 330 nm) using a spectrometer based on a MDR-23 monochromator and a PMT-100 photomultiplier tube. The plastic electrolytic cell was manufactured to provide transparent and conductive contact with the samples. The test sample was placed between the metal anode and a 5 mm diameter hole, which provided contact between the emitting layer and the electrolyte. The front part of the electrolytic cell is equipped with a JGS1 quartz glass. A 1 M Na_2SO_4 aqueous solution was used as an electrolyte. The SiO_2-electrolyte-quarz-air system provides 93–95 % light transmittance in the wavelength range of 330–705 nm. The measurements were performed at a small solid angle (0.02 sr). Therefore, the effect of the electrolytic cell on the radial distribution of intensity was less than 1 %, according to our estimates. EL spectra were recorded in galvanostatic mode with a positive bias applied to the silicon substrate (forward bias). Such regime of the EL measurement did not result in dielectric layer etching, and the use of p-type silicon made it possible to create a region enriched with majority charge carriers – holes at the Si-SiO_2 interface in silicon. [24] EL spectra were recorded under constant injection current density through the sample 50 μA cm^{-2} using an IPPP-1/6 semiconductor parameter analyzer. The light-emitting spot diameter was 5 mm. The EL spectra were obtained in the absolute values of the spectral radiant exitance ($M_{e\lambda}$). A description of the methodology for obtaining EL spectra in absolute values and calibrating spectrometer is given in the Supplemental file. The dependence of radiant exitance on current density $M_e(j)$ and the average electric field strength $M_e(F)$ were obtained via simultaneous recording the EL intensity and the current – voltage characteristics.

3. Results and discussion

Fig. 2 demonstrates XTEM images of the Sn-implanted and annealed silica layers.

The thickness of the annealed implanted layers decreased with the increasing fluence due to radiative sputtering during high-fluence implantation. The thicknesses were 131, 128 and 92 nm for the samples implanted with fluences of 2.5×10^{16}, 5×10^{16} and 1×10^{17} cm^{-2}, respectively. The lattice spacings of the nanoparticles were determined

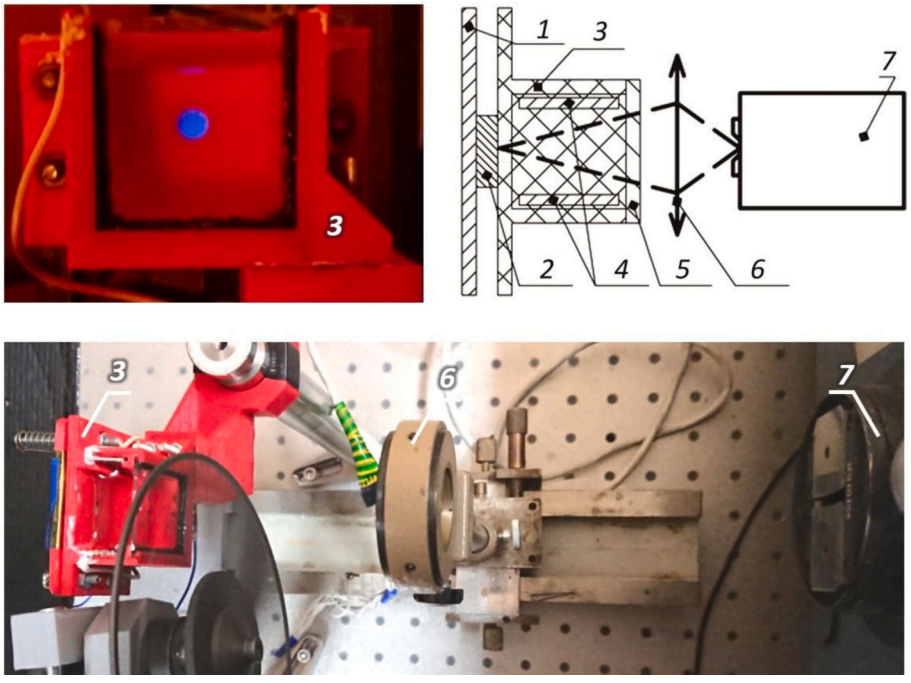

Fig. 1. Scheme of setup for EL measurements: 1 – anode, 2 – sample, 3 – electrochemical cell, 4 – cathodes, 5 – quartz glass, 6 – quartz lens, 7 – monochromator.

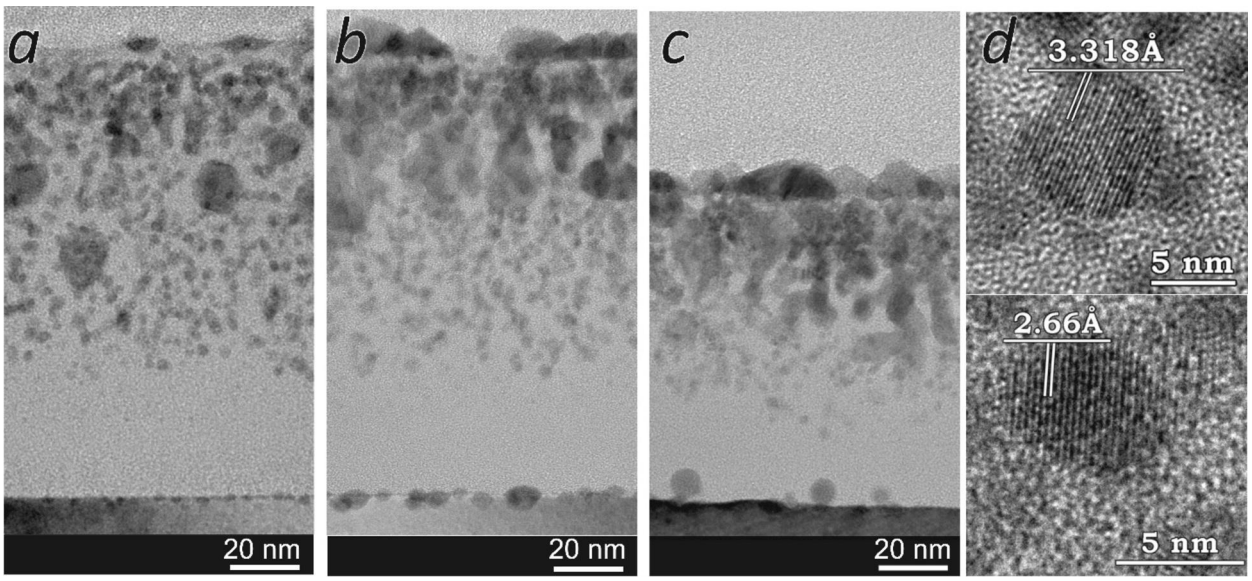

Fig. 2. Cross-sectional images of the annealed silica samples Sn-implanted with fluences of 2.5×10^{16} (a), 5×10^{16} (b) and 1×10^{17} cm^{-2} (c) and enlarged HRTEM image of separate nanocrystals (d).

from the HRTEM images (Fig. 2d). The measured interplanar distances of 0.33 nm and 0.26 nm agrees with the (1 1 0) and (1 0 1) lattice fringes of tetragonal SnO_2. With increasing fluence, the formation of dendrites and merged nanoparticles becomes more pronounced. Besides, in the case of the highest Sn fluence, the formation of β-Sn nanocrystals at the SiO_2/Si interface was revealed.

Fig. 3a shows the hysteresis of the current–voltage characteristics (*I–V*) of the sample implanted with the lowest fluence. The direction of measurement is shown by arrows. A current flowing through the sample results in a shift in the *I–V* characteristic to the region of strong fields due to charge accumulation on traps in the implanted layers. The *I–V* characteristic branch measured with an increase in the anode potential has distortions caused by charge accumulation on traps. Subsequent measurements of the *I–V* characteristics of the samples did not lead to significant distortions of the characteristics. Fig. 3b shows the I-V characteristics of implanted and annealed samples, measured in a state with filled traps.

To clarify the mechanisms of charge carrier transport in the implanted and annealed SiO_2 layers, measurements of the current–voltage characteristics were carried out in a state with filled traps. (Fig. 3b). As can be seen, all the *I–V* characteristics can be divided into three sections with different slopes: the region of weak (I), medium (II), and high (III) fields. The carrier transport mechanisms in each section may differ. The obtained current–voltage characteristics are not straightened in the coordinates corresponding to the Fowler-Nordheim, Schottky and Poole–Frenkel models. The nonuniform distribution of nanoprecipitates over the depth of the implanted layers complicates the interpretation of charge carrier transport mechanisms. The current flow at a voltage less than 10 V (~1 MV cm^{-1}) indicates that the transfer of charge carriers in the implanted layers occurs via deep level states in the band gap (Baraban, 1988). Such states can be related to three-coordinated silicon atoms, non-bridging oxygen atoms, and peroxyl radical (Robertson, 1985; Shaposhnikov et al., 2002; Baraban and Dmitriev, 2021). Charge carrier transfer can also occur via defect levels related with Sn atoms (Rebohle et al., 2000). In the region of strong fields, the increase in current has superexponential dependence, which can be caused by the avalanche multiplication of charge carriers (Baraban, 1988). As can be seen, an increase in tin ion fluence leads to a shift in the I-V characteristics to the region of weak fields. This is due to both a decrease in the SiO_2 thickness via ion sputtering and an increase in the conductivity of the implanted layers.

Fig. 4a shows the EL spectra of the annealed samples. The EL spectra were obtained as absolute values of the spectral radiant exitance ($M_{e\lambda}$). The inset in Fig. 4a depicts an image of a sample emitted brightly in the violet range. The intense violet band at 3.21 eV dominates in the spectra. Its intensity decreases as the Sn concentration increases in silica.

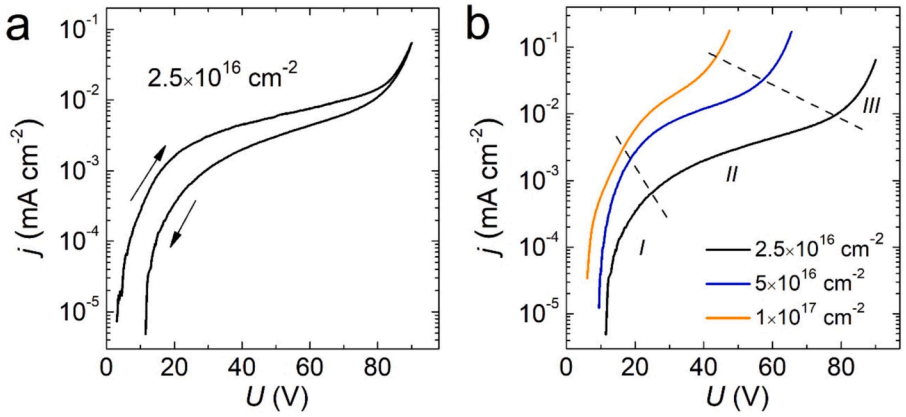

Fig. 3. Voltage dependence on time (a) and current–voltage characteristics (b) of the annealed Sn-implanted silica samples.

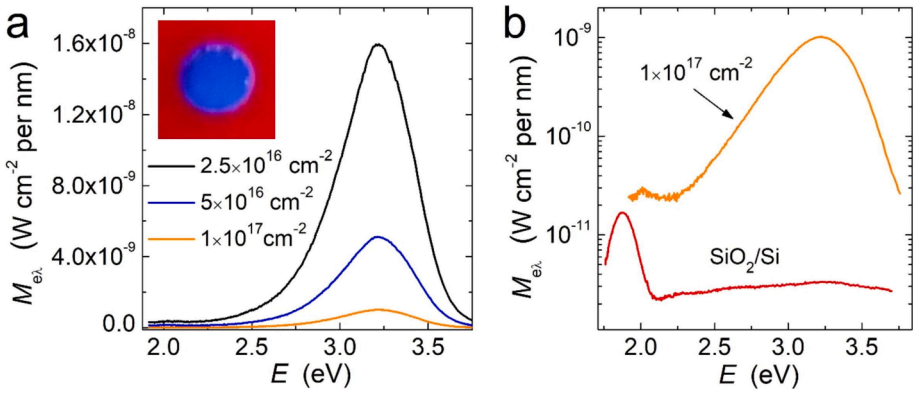

Fig. 4. EL spectra (spectral radiant exitance) of the annealed Sn-implanted silica (a) and comparison of the EL spectra of the pristine silica sample (SiO_2(130 nm)/Si) and the annealed silica sample Sn-implanted with fluence of 1×10^{17} cm^{-2} (b). All spectra were measured at $j_0 = 50$ μA cm^{-2}.

According to (Romanov et al., 2022), the EL band at 3.21 eV can be attributed to radiative recombination in SnO_2 nanocrystals. The rapid decrease in EL intensity with the implantation fluence can be attributed to an increase in the concentration of nonradiative recombination centers as well as an increase of the current flowing through deep localized states in the implanted SiO_2 layers and not participating in the EL excitation processes (Romanov et al., 2022).

Fig. 4b shows the EL spectra of the sample implanted with the maximum fluence and annealed compared with the pristine SiO_2/Si structure with the same SiO_2 thickness. The EL spectrum of the pristine silica layer is dominates by a low-intensity band with a maximum at 1.9 eV, which can be attributed to the presence of silanol groups (Si–OH) in the silicon oxide (Baraban et al., 2019; Romanov et al., 2018). As can be seen, Sn implantation with subsequent annealing results in an increase of EL intensity by two orders of magnitude.

Fig. 5a shows the dependence of radiant exitance on the current density $M_e(j)$ for the implanted and annealed samples. The inset depicts an enlarged area of the $M_e(j)$ characteristic at low j for the sample implanted with the lowest fluence of 2.5×10^{16} cm^{-2}. As can be seen, the $M_e(j)$ dependences are nonlinear at current densities up to 5 μA•cm^{-2}. The $M_e(j)$ characteristics become quasilinear at current densities greater than 10 μA•cm^{-2}.

The radiant exitance ($M_e(j_0)$) was determined by integrating the spectral radiant exitance in the range of 330 – 710 nm at a current density of 50 μA cm^{-2}. $M_e(j)$ dependences were determined as:

$$M_e(j) = \frac{I(j)}{I_0}\int M_{e\lambda}\,d\lambda = \frac{I(j)}{I_0}M_e(j_0) \tag{1}$$

where $I(j)$ is the EL intensity measured at j current density, I_0 is the EL intensity measured at $j_0 = 50$ μA cm^{-2}, λ is the wavelength. The EL signal was measured at a photon energy of 3.2 eV. Since our experiments did not reveal any differences in the EL spectra measured at various currents, Eq. (1) can be considered accurate.

External quantum efficiency is defined as the ratio of the number of emitted photons to the number of passed charge carries. The flux density of photons emitted per second by the surface of the sample can be determined by the expression:

$$N_p = \int \frac{M_{e\lambda}}{E_\lambda e}\,d\lambda = (ehc)^{-1}\int M_{e\lambda}\lambda\,d\lambda \tag{2}$$

where E_λ is the photon energy at the wavelength λ in eV, e is the electron charge, h is Planck's constant in eV·s, and c is the speed of light.

The density of electrons passing through the sample per second was determined as follows:

$$N_e(j) = \frac{j}{e} \tag{3}$$

Based on equations (1) – (3), we obtain the following expression for the external quantum yield:

$$\eta_{EQE}(j) = \frac{N_p(j)}{N_e(j)} = \frac{I(j)}{I_0\,jhc}\int_{330}^{710} M_{e\lambda}\lambda\,d\lambda \tag{4}$$

where $M_{e\lambda}$ is the EL spectrum obtained at $j_0 = 50$ μA cm^{-2} (see Fig. 2a).

Fig. 5b shows the dependence of the external quantum efficiency of the EL on the current density for the samples implanted with different fluences. The EQE rapidly increased at low current densities (up to 10 μA cm^{-2}). For j greater than 10 μA cm^{-2}, the function EQE(j) is saturated. Such type of $M_e(j)$ and EQE(j) dependences indicates that the fraction of charge carriers involved in the radiative recombination

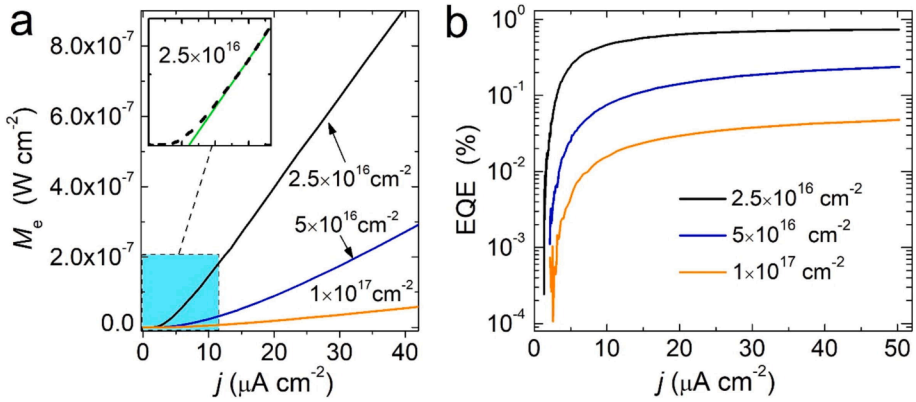

Fig. 5. Radiant emittance of the EL band at 3.21 eV (M_e) (a) and external quantum efficiency (b) as functions of current density for the annealed Sn-implanted silica samples.

increases with increasing current flowing through the samples. The EQE values obtained by passing a current density of 50 μA cm^{-2} through the samples are given in Table 1.

The maximum EQE of the pristine SiO_2 layer is 1.3 × 10^{-5}. Sn implantation with subsequent annealing significantly increased EQE. It should be noted that the EQE increased with decreasing the Sn^+ fluence. The maximum value of the EQE is ~ 0.7 % for the sample implanted with the lowest fluence. The relatively low quantum efficiency indicates that the current flowing through the samples is mainly due to the transfer of charge carriers not involved in radiative recombination processes. Threshold values for current densities (j_{min}) under EL excitation are given in Table 1. It can be seen that j_{min} increases with the implantation fluence. The absence of EL signal at low currents can be attributed to nonradiative charge-carrier transport through deep level states in SiO_2. At low current values, the electric field strength is low (less than 2 MV cm^{-1}), and the carrier energy is not enough to excite an EL processes. The increase of j_{min} as well as the decrease in EQE with the fluence increase can be explained by an increase in the concentration of defects that form deep level states in SiO_2 matrix.

The dependence of the EL radiant exitance on the average electric field strength $M_e(F)$ was studied to determine the mechanisms of charge carrier transport responsible for violet light emission. The EL signal appeared at an electric field strength greater than 2 MV cm^{-1}. Fig. 6a shows the experimental $M_e(F)$ characteristics in semi-logarithmic coordinates for the samples implanted with different fluences. In contrast to the current–voltage characteristics (Fig. 3b) (), the $M_e(F)$ characteristics in semi-logarithmic coordinates exhibit linear dependence. This dependence is typical for dielectrics with a high trap concentration. For such materials, carrier transport is described by the Poole–Frenkel mechanism (Nasyrov and Gritsenko, 2013; Hill, 1971) or by tunneling between traps (Odzaev et al., 2020). The Poole–Frenkel effect arises from the emission of charge carriers trapped at defect levels and subsequent transition into the conduction band (for electrons) or the valence band (for holes). Fig. 6b shows the experimental $M_e(F)$ characteristics in the Poole-Frenkel coordinates.

Taking into account tunneling between traps, the experimental characteristics of $M_e(F)$ (Fig. 6 a) are well approximated at low and medium luminescence intensities (up to 10^{-6} W cm^{-2}) by following expression (Gismatulin et al., 2019):

$$M_e = A_t \sinh\left(\frac{eN_{tr}^{-1/3}F}{2kT}\right) \quad (5)$$

where A_t is the parameter depending on the optical and electrical properties of the sample and N_{tr} is the trap concentration.

The values of N_{tr} determined by this approximation are also given in Table 1. N_{tr} parameter characterizes the concentration of traps that provide the transfer of carriers to luminescence centers. A decrease in the N_{tr} with an increase in the fluence may indicate a reduction in the number of tunneling events between traps. SiO_2 implantation with high Sn^+ fluences as 5 × 10^{16} and 1 × 10^{17} cm^{-2} and subsequent annealing leads to the formation of merged nanoparticles and dendrites. Charge carriers can move without tunneling over long distances along such dendrites (Zatsepin et al., 2012). Then, the number of traps involved in the charge carriers transport to luminescence centers is less than in the sample implanted with a fluence of 2.5 × 10^{16} cm^{-2} (Nasyrov and Gritsenko, 2013). The large value of N_{tr} for the sample implanted with a fluence of 2.5 × 10^{16} cm^{-2} indicates tunneling through the localized states. In this case, to obtain an intense EL a higher voltage is required.

Table 1
Threshold current densities for EL appearance, EQEs after passing through the samples j = 50 μA cm^{-2}, calculated trap concentrations N_{tr}, and dielectric permittivity.

Sn fluences, cm^{-2}	j_{min}, μA•cm^{-2}	EQE, %	N_{tr} × 10^{20}, cm^{-3}	ε, arb. u.
2.5 × 10^{16}	0.9	0.74	4.3	6.4
5 × 10^{16}	2.0	0.24	2.6	6.9
1 × 10^{17}	2.7	0.05	2.4	7.9

Classical Poole-Frenkel law is described by the equation (Hill, 1971):

$$M_e = A_{P-F} F \exp\left(\frac{\beta_{P-F}\sqrt{F}}{kT}\right); \beta_{P-F} = \sqrt{\frac{e^3}{\pi\varepsilon_0\varepsilon}} \quad (6)$$

where $A_{P\text{-}F}$ is a parameter depending on the optical and electrical properties of the sample, $\beta_{P\text{-}F}$ is the Frenkel constant, ε is the dielectric permittivity of the implanted and annealed layers.

As shown in Fig. 6 b, the experimental characteristics of $M_e(F)$ can be well approximated by the classical Poole-Frenkel law at low and medium luminescence intensities. The values of ε determined by this approximation are also given in Table 1. It is known that the dielectric permittivity of SiO_2 is 3.9, and this parameter is greater than 10 for SnO_2 films (Ahmad et al., 2019). As can be seen in the Table 1, the dielectric permittivity increases from 6.4 to 7.9 with increasing implantation dose. This is probably due to an increase in the SnO_2 phase content in the implanted layers.

In conclusion, let us discuss charge carrier transport through SiO_2-SnO_2 nanocomposite. The total current flowing through the sample consists of 'shunt' current and current produces excitation of luminescence centers (j_{EL}). In the case of a weak electric field (region I in Fig. 2b), charge carriers are transported through deep level states, with j_{EL} = 0. An increase in the electric field (region II in Fig. 2b) leads to the appearance of a current j_{EL}. Fig. 7 shows the band diagram of the Si/SiO_2/SnO_2/SiO_2/electrolyte system at forward bias. It is assumed that violet emission is related to the radiative recombination of electrons localized at the oxygen-vacancy levels in SnO_2 nanocrystals with holes in the valence band (Romanov et al., 2022). Electrons from the electrolyte are injected into the silicon oxide and trapped at deep defect levels (1). Then, the injected electrons tunnel between traps (2) and are transferred to the conduction band of the SnO_2 nanocrystal. Then, electrons from the SnO_2 conduction band are captured by oxygen vacancies (V_O^+ or V_O^{2+}). The hole transfer to the SnO_2 valence band can be carried out by tunneling from silicon into the shallow trap levels (3) and subsequent transition into the valence band of SiO_2 via the Poole–-Frenkel effect (4). Mechanism 3 is possible when the electric field strength is sufficient to form a thin tunnel barrier between the silicon valence band and the trap energy level. Thus, the appearance of an EL signal at a field strength of ~ 2 MV cm^{-1} can be explained by a decrease of the potential barrier and tunneling holes from silicon into the shallow trap levels in SiO_2 with subsequent hole transport to the SnO_2 valence band.

4. Conclusions

SiO_2 layers with embedded SnO_2 nanocrystals were synthesized by Sn ion implantation of SiO_2/Si structures at different fluences with subsequent annealing in air (900 °C, 60 min). The fabricated SiO_2:SnO_2/p-Si structures exhibited bright violet electroluminescence with a maximum at 3.21 eV at a forward bias that could be attributed to the radiative recombination in SnO_2 nanocrystals. The sample implanted with the lowest fluence of 2.5 × 10^{16} cm^{-2} have exhibited the lowest threshold current density (0.9 μA•cm^{-2}) for EL appearance and the highest external quantum efficiency (0.7 %). The deterioration of the light emission characteristics with the fluence increase is attributed to the increase in defect concentration in SiO_2. In turn, it increases the possibility of charge carrier transport through the implanted layer without EL excitation. A model of charge carriers transport through the implanted layers has been suggested. At current densities below 5 μA cm^{-2}, the most of charge carriers are tunneling to deep levels in SiO_2 without EL excitation. On the basis of the analysis of the dependence of EL radiant exitance on electric field strength, we can conclude that charge carrier transport to luminescent centers occurs according to the Poole–Frenkel mechanism or tunneling between traps. We believe that

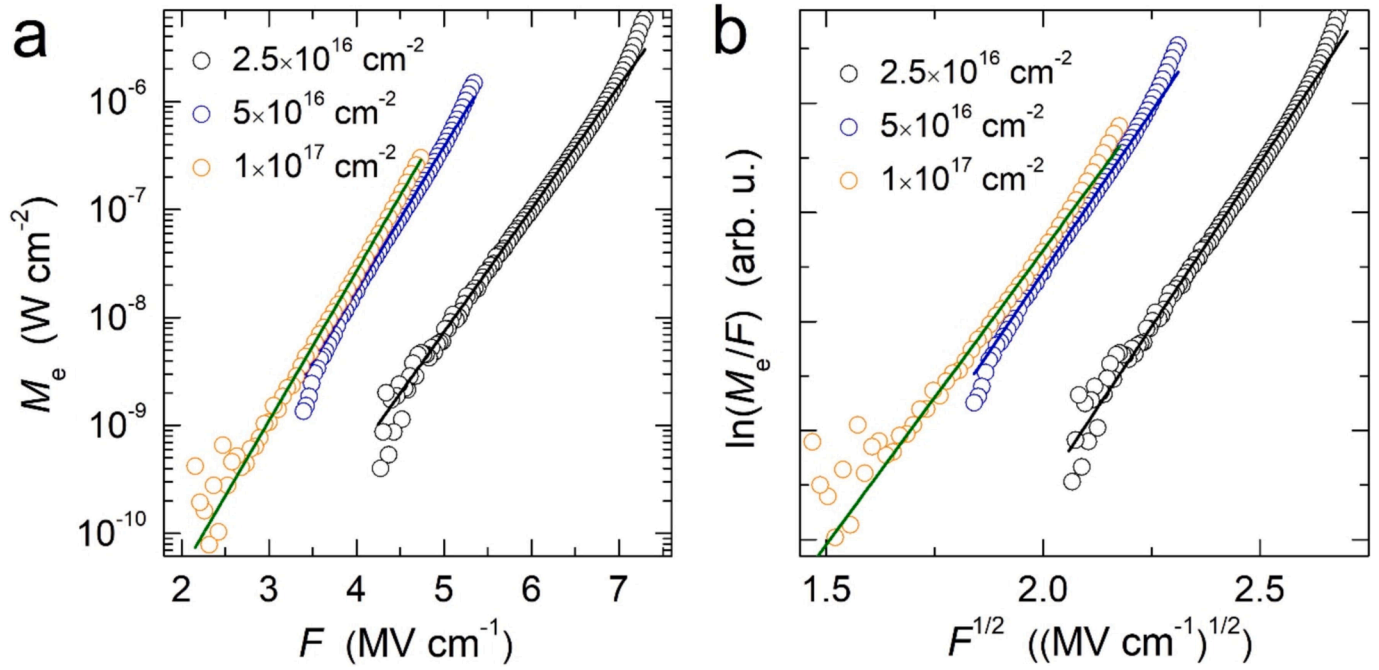

Fig. 6. Radiant exitance of the EL band at 3.21 eV (M_e) in semi-logarithmic scale as a function of the average electric field strength (F) (a) and the same presented in coordinates corresponding to the Poole–Frenkel law (b) for the annealed Sn-implanted samples.

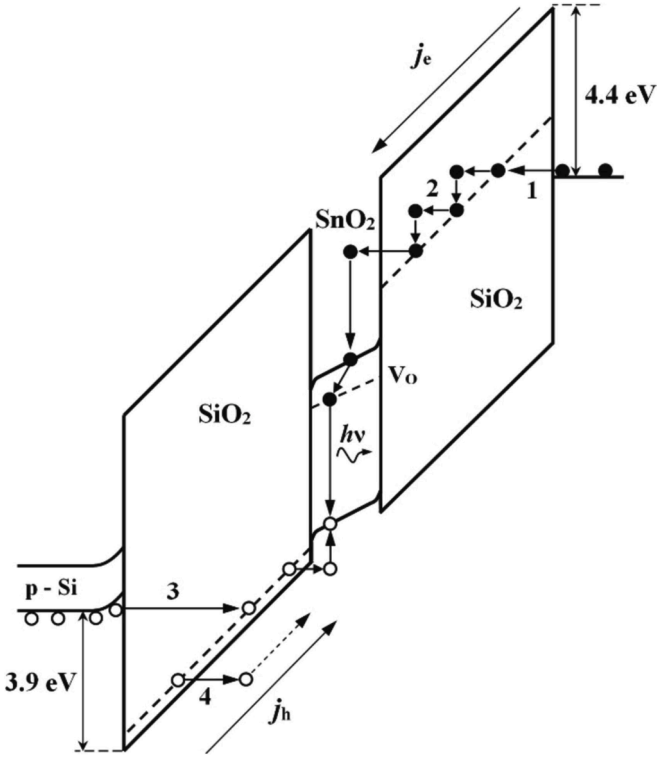

Fig. 7. Band diagram of the electrolyte/SiO_2/SnO_2/SiO_2/p-Si system and charge carrier transport mechanisms: 1 – tunneling of charge carriers to deep defect levels; 2 – tunneling between traps; 3 – tunneling holes into shallow trap levels; 4 – hole transport via the Poole–Frenkel effect.

this study will provides a way to further develop silicon-compatible LEDs using SnO_2 nanocrystals embedded in SiO_2/Si structures.

CRediT authorship contribution statement

Ivan Romanov: Writing – original draft, Methodology, Investigation, Conceptualization. **Irina Parkhomenko:** Visualization, Investigation, Data curation, Conceptualization. **Liudmila Vlasukova:** Writing – original draft, Supervision, Funding acquisition, Data curation, Conceptualization. **Elke Wendler:** Investigation. **Fadei Komarov:** Supervision, Conceptualization.

Declaration of competing interest

The authors declare that they have no known competing financial interests or personal relationships that could have appeared to influence the work reported in this paper.

Acknowledgment

This work was supported by the Belarusian state program of scientific research 'Photonics and electronic for innovations' (projects 3.8.1, SR No 20212595).

Appendix A. Supplementary data

Supplementary data to this article can be found online at https://doi.org/10.1016/j.rio.2024.100750.

Data availability

Data will be made available on request.

References

Ahmad, N., Khan, S., Nizam Ansari, M.M., 2019. Exploration of Raman spectroscopy, dielectric and magnetic properties of (Mn, Co) co-doped SnO2 nanoparticles. Phys. B Condens. Matter. 558, 131–141. https://doi.org/10.1016/j.physb.2019.01.044.

Arai, N., Tsuji, H., Hattori, M., Ohsaki, M., Kotaki, H., Ishibashi, T., Gotoh, Y., Ishikawa, J., 2009. Luminescence properties of Ge implanted SiO2: Ge and GeO2: Ge films. Appl. Surf. Sci. 256, 954–957. https://doi.org/10.1016/j.apsusc.2009.05.062.

Baraban, A.P., 1988. Electronics of SiO2 layers on silicon. St. Petersburg University Press, Leningrad.

Baraban, A.P., Dmitriev, V.A., 2021. Luminescence of insulator layers on silicon excited by electrons. Phys. Complex Syst. 2, 9–14. https://doi.org/10.33910/2687-153X-2021-2-1-9-14.

Baraban, A.P., Samarin, S.N., Prokofiev, V.A., Dmitriev, V.A., Selivanov, A.A., Petrov, Y., 2019. Luminescence of SiO2 layers on silicon at various types of excitation. J. Lumin. 205, 102–108. https://doi.org/10.1016/j.jlumin.2018.09.009.

Bregolin, F.L., Behar, M., Sias, U.S., Reboh, S., Lehmann, J., Rebohle, L., Skorupa, W., 2009. Electroluminescence induced by Ge nanocrystals obtained by hot ion implantation into SiO2. J. Appl. Phys. 106. https://doi.org/10.1063/1.3262627.

Cho, Y., Jeon, M.S., Jang, H., Lee, H.S., Kim, D.R., 2021. High quality GaN tetrapodal structures hetero-integrated on 3D Si surfaces. Appl. Surf. Sci. 565, 150584. https://doi.org/10.1016/j.apsusc.2021.150584.

T. Fujimoto, K. Gi, S. Bigoni, M. Celebrano, M. Finazzi, G. Ferrari, T. Shinada, E. Prati, T. Tanii, Electroluminescence of Er:O-doped nano pn diode in silicon-on-insulator and its current-voltage characteristics at room temperature, in: 2020 IEEE Silicon Nanoelectron. Work., IEEE, 2020: pp. 123–124. https://doi.org/10.1109/SNW50361.2020.9131655.

Gismatulin, A.A., Kruchinin, V.N., Gritsenko, V.A., Prosvirin, I.P., Yen, T.-J., Chin, A., 2019. Charge transport mechanism of high-resistive state in RRAM based on SiO x. Appl. Phys. Lett. 114. https://doi.org/10.1063/1.5074116.

Gong, K., Kelley, D.F., Kelley, A.M., 2016. Resonance Raman Spectroscopy and Electron-Phonon Coupling in Zinc Selenide Quantum Dots. J. Phys. Chem. c. 120, 29533–29539. https://doi.org/10.1021/acs.jpcc.6b12202.

Hikosaka, T., Yoshida, H., Sugiyama, N., Nunoue, S., 2014. Reduction of threading dislocation by recoating GaN island surface with SiN for high-efficiency GaN-on-Si-based LED. Phys. Status Solidi c. 11, 617–620. https://doi.org/10.1002/pssc.201300441.

Hill, R.M., 1971. Poole-Frenkel conduction in amorphous solids. Philos. Mag. 23, 59–86. https://doi.org/10.1080/14786437108216365.

Huang, S., Cho, E.-C., Conibeer, G., Green, M.A., 2011. Structural and photoluminescence properties of superlattice structures consisting of Sn-rich SiO2 and stoichiometric SiO2 layers. Thin Solid Films. 520, 641–645. https://doi.org/10.1016/j.tsf.2011.08.027.

Huang, Y., Saito, K., Tanaka, T., Guo, Q., 2021. Realization of red electroluminescence from Ga2O3:Eu/Si based light-emitting diodes. Superlattices Microstruct. 150, 106814. https://doi.org/10.1016/j.spmi.2021.106814.

O. Jambois, J. Carreras, A. Pérez-Rodríguez, B. Garrido, C. Bonafos, S. Schamm, G. Ben Assayag, Field effect white and tunable electroluminescence from ion beam synthesized Si- and C-rich SiO2 layers, Appl. Phys. Lett. 91 (2007). https://doi.org/10.1063/1.2807281.

Jiang, S., Ren, Z., Gong, S., Yin, S., Yu, Y., Li, X., Xu, G., Shen, G., Han, G., 2014. Tunable photoluminescence properties of well-aligned ZnO nanorod array by oxygen plasma post-treatment. Appl. Surf. Sci. 289, 252–256. https://doi.org/10.1016/j.apsusc.2013.10.146.

M.S.I. Koubisy, A.F. Zatsepin, D.Y. Biryukov, T. V. Shtang, N. V. Gavrilov, Optical absorption and luminescence of oxygen-deficient centers in silica glass implanted with 30 keV RE-ions, in: 2020: p. 030020. https://doi.org/10.1063/5.0032286.

Lee, M., Shin, Y., Lee, H.U., Jeong, Y., Hahm, M.G., Kim, J., 2020. Origin of high quantum efficiency in Si-based homoepitaxial InGaN/GaN light-emitting diodes. J. Phys. d. Appl. Phys. 53, 375102. https://doi.org/10.1088/1361-6463/ab9330.

Li, C., Ouyang, L., Li, X., Xu, C., Xie, J., Li, Y., Tang, S., Ye, S., Yang, J., Wang, R., Qiu, F., Wang, J., Yang, Y., Wang, C., 2021. Optical properties of multiple energy silicon implantation in silicon films using silicon-on-insulator targets. Opt. Mater. (amst). 116, 111065. https://doi.org/10.1016/j.optmat.2021.111065.

Li, Y., Yin, W., Deng, R., Chen, R., Chen, J., Yan, Q., Yao, B., Sun, H., Wei, S.-H., Wu, T., 2012. Realizing a SnO2-based ultraviolet light-emitting diode via breaking the dipole-forbidden rule. NPG Asia Mater. 4, e30–e. https://doi.org/10.1038/am.2012.56.

Liu, Y., Jiang, M., Tang, K., Ma, K., Wu, Y., Ji, J., Kan, C., 2020. Plasmon-enhanced high-performance Si-based light sources by incorporating alloyed Au and Ag nanorods. CrystEngComm. 22, 6106–6115. https://doi.org/10.1039/D0CE00823K.

Lopes, J.M.J., Zawislak, F.C., Fichtner, P.F.P., Lovey, F.C., Condó, A.M., 2005. Effect of annealing atmosphere on the structure and luminescence of Sn-implanted SiO2 layers. Appl. Phys. Lett. 86. https://doi.org/10.1063/1.1849855.

Lopes, J.M.J., Kremer, F., Fichtner, P.F.P., Zawislak, F.C., 2006. Correlation between structural evolution and photoluminescence of Sn nanoclusters in SiO2 layers. Nucl. Instruments Methods Phys. Res. Sect. B Beam Interact. with Mater. Atoms. 157–160. https://doi.org/10.1016/j.nimb.2005.08.013.

Martinelli, L., Grilli, E., Guzzi, M., Grimaldi, M.G., 2003. Room-temperature electroluminescence of ion-beam-synthesized β-FeSi2 precipitates in silicon. Appl. Phys. Lett. 83, 794–796. https://doi.org/10.1063/1.1593815.

Nasyrov, K.A., Gritsenko, V.A., 2013. Transport mechanisms of electrons and holes in dielectric films. Uspekhi Fiz. Nauk. 183, 1099–1114. https://doi.org/10.3367/UFNr.0183.201310h.1099.

Nikolskaya, A., Korolev, D., Tereshchenko, A., Pavlenkov, V., Nagornykh, S., Belov, A., Vasiliev, V., Mikhaylov, A., Tetelbaum, D., 2020. Temperature dependence of dislocation-related photoluminescence (D1) of self-implanted silicon subjected to additional boron implantation. Nucl. Instruments Methods Phys. Res. Sect. B Beam Interact. with Mater. Atoms. 472, 32–35. https://doi.org/10.1016/j.nimb.2020.03.032.

Odzaev, V.B., Panfilenka, A.K., Pyatlitski, A.N., Prasalovich, U.S., Kovalchuk, N.S., Soloviev, Y.A., Filipenia, V.A., Shestovski, D.V., 2020. Influence of nitrogen ion implantation on the electrophysical properties of the gate dielectric of power MOSFETs. J. Belarusian State Univ. Phys. 55–64. https://doi.org/10.33581/2520-2243-2020-3-55-64.

Rebohle, L., von Borany, J., Fröb, H., Skorupa, W., 2000. Blue photo- and electroluminescence of silicon dioxide layers ion-implanted with group IV elements. Appl. Phys. B Lasers Opt. 71, 131–151. https://doi.org/10.1007/PL00006966.

Rebohle, L., von Borany, J., Skorupa, W., Fröb, H., Niedermeier, S., 2000. Strong photoluminescence of Sn-implanted thermally grown SiO2 layers. Appl. Phys. Lett. 77, 969–971. https://doi.org/10.1063/1.1289032.

Rebohle, L., von Borany, J., Fröb, H., Gebel, T., Helm, M., Skorupa, W., 2002. Ion beam synthesized nanoclusters for silicon-based light emission. Nucl. Instruments Methods Phys. Res. Sect. B Beam Interact. with Mater. Atoms. 188, 28–35. https://doi.org/10.1016/S0168-583X(01)01004-7.

Rebohle, L., Berencén, Y., Wutzler, R., Braun, M., Hiller, D., Ramírez, J.M., Garrido, B., Helm, M., Skorupa, W., 2014. The electroluminescence mechanism of Er3+ in different silicon oxide and silicon nitride environments. J. Appl. Phys. 116. https://doi.org/10.1063/1.4896588.

Robertson, J., 1985. Defect mechanisms in a-SiO2. Philos. Mag. b. 52, 371–377. https://doi.org/10.1080/13642818508240608.

Romanov, I., Komarov, F., Milchanin, O., Vlasukova, L., Parkhomenko, I., Makhavikou, M., Wendler, E., Mudryi, A., Togambayeva, A., 2019. Structural Evolution and Photoluminescence of SiO 2 Layers with Sn Nanoclusters Formed by Ion Implantation. J. Nanomater. 2019, 1–9. https://doi.org/10.1155/2019/9486745.

Romanov, I., Komarov, F., Parkhomenko, I., Vlasukova, L., Makhavikou, M., Milchanin, O., Wendler, E., van Vuuren, A., Neethling, J., 2022. Fluence effect on photo- and electroluminescence of silica layers implanted with Sn+ ions. Mater. Lett. 308, 131070. https://doi.org/10.1016/j.matlet.2021.131070.

Romanov, I.A., Vlasukova, L.A., Komarov, F.F., Parkhomenko, I.N., Kovalchuk, N.S., Mohovikov, M.A., Mudryi, A.V., Milchanin, O.V., 2018. Photo- and electroluminescence of oxide-nitride-oxide-silicon structures for silicon-based optoelectronics. Dokl. Natl. Acad. Sci. Belarus. 62, 546–554. https://doi.org/10.29235/1561-8323-2018-62-5-546-554.

Shaposhnikov, A.V., Gritsenko, V.A., Zhidomirov, G.M., Roger, M., 2002. Hole trapping on the twofold-coordinated silicon atom in SiO2. Phys. Solid State. 44, 1028–1030. https://doi.org/10.1134/1.1485002.

Shcheglov, K.V., Yang, C.M., Vahala, K.J., Atwater, H.A., 1995. Electroluminescence and photoluminescence of Ge-implanted Si/SiO2/Si structures. Appl. Phys. Lett. 66, 745–747. https://doi.org/10.1063/1.114080.

Tagliente, M.A., Bello, V., Pellegrini, G., Mattei, G., Mazzoldi, P., Massaro, M., 2009. SnO 2 nanoparticles embedded in silica by ion implantation followed by thermal oxidation. J. Appl. Phys. 106. https://doi.org/10.1063/1.3257157.

Wu, S., Zhang, L., Wan, R., Zhou, H., Lee, K.H., Chen, Q., Huang, Y.-C., Gong, X., Tan, C. S., 2023. Ge 0.92 Sn 0.08 /Ge multi-quantum-well LEDs operated at 2-μm-wavelength on a 12-inch Si substrate. Photonics Res. 11. https://doi.org/10.1364/PRJ.491763.

Xiang, G., Zhou, Y., Peng, W., Zhang, J., Liu, Y., Zhang, J., Yue, Z., Zhang, X., Song, C., Ding, B., Jin, Y., Wang, P., Wang, H., Zhao, Y., 2023. Vacuum-deposited perovskite CsPbBr 3 thin-films for temperature-stable Si based pure-green all-inorganic light-emitting diodes. Ceram. Int. 49, 21624–21633. https://doi.org/10.1016/j.ceramint.2023.03.298.

Zatsepin, A.F., Buntov, E.A., Kortov, V.S., Pustovarov, V.A., Fitting, H.-J., Schmidt, B., Gavrilov, N.V., 2012. Low-temperature photoluminescence of ion-implanted SiO2: Sn + films and glasses. J. Surf. Investig. X-Ray, Synchrotron Neutron Tech. 6, 668–672. https://doi.org/10.1134/S1027451012080198.

Zatsepin, D.A., Zatsepin, A.F., Boukhvalov, D.W., Kurmaev, E.Z., Gavrilov, N.V., 2016. Sn-loss effect in a Sn-implanted a-SiO2 host-matrix after thermal annealing: A combined XPS, PL, and DFT study. Appl. Surf. Sci. 367, 320–326. https://doi.org/10.1016/j.apsusc.2016.01.126.

J.F. Ziegler, M.D. Ziegler, J.P. Biersack, SRIM - The stopping and range of ions in matter (2010), Nucl. Instruments Methods Phys. Res. Sect. B Beam Interact. with Mater. Atoms. 268 (2010) 1818–1823. https://doi.org/10.1016/j.nimb.2010.02.091.